Angular quasi-phase-matching experiments and determination of accurate Sellmeier equations for 5%MgO:PPLN

Pierre Brand, Benoit Boulanger, Patricia Segonds, Yannick Petit, Corinne Felix, Bertrand Ménaert, Takunori Taira, Hideki Ishizuki

Angular quasi-phase-matching experiments and determination of accurate Sellmeier equations for 5%MgO:PPLN

Pierre Brand,[1] Benoît Boulanger,[1,*] Patricia Segonds,[1] Yannick Petit,[1,2] Corinne Félix,[1] Bertrand Ménaert,[1] Takunori Taira,[3] and Hideki Ishizuki[3]

[1]*Institut Néel CNRS/UJF, 25 rue des Martyrs, BP 166, F38402 Grenoble Cedex 9, France*
[2]*Université de Genève, 20 rue de l'Ecole de Médecine, Genève, Suisse*
[3]*Institute for Molecular Science, 38 Nishigonaka Myodaili Okazaki 444-8585 Japan*
**Corresponding author: benoit.boulanger@grenoble.cnrs.fr*

We validated the theory of angular quasi-phase-matching (AQPM) by performing measurements of second-harmonic generation and difference-frequency generation. A nonlinear least-squares fitting of these experimental data led to refine the Sellmeier equations of 5%MgO:PPLN that are now valid over the complete transparency range of the crystal. We also showed that AQPM exhibits complementary spectral ranges and acceptances compared with birefringence phase matching.

Quasi-phase-matching in periodically poled materials is today the most promising configuration for achieving efficient three-wave nonlinear parametric interactions [1–4]. However, the difficulty of fabricating thick samples usually forbids the use of large beams, thus restricting the incident energy because of damage threshold limitations. Recent advances led for the first time to few-millimeters-thick periodically poled $LiNbO_3$ (PPLN) slabs, allowing the use of pump laser beams with larger aperture, and so with higher energy [5]. Moreover, such large samples offer the possibility to consider quasi-phase-matching at any angle with respect to the grating vector while keeping a reasonable interaction length. We called this configuration angular quasi-phase-matching (AQPM) [6].

We present here the first (to our knowledge) second-harmonic generation (SHG) and difference-frequency generation (DFG) measurements of AQPM performed in 5%MgO:PPLN in order to validate the theory. From these data we also establish reliable Sellmeier equations that are valid over the entire transparency range of the crystal. Finally, we discuss the interest of AQPM from calculations.

We considered a periodically poled medium, where the grating periodicity Λ is oriented along the x axis of the dielectric frame of the crystal. AQPM is optimized when momentum conservation is achieved, which is the case when the three interacting waves propagate in directions that are solutions of the following equation [6]:

$$\frac{n_3(\theta,\phi)}{\lambda_3}-\frac{n_2(\theta,\phi)}{\lambda_2}-\frac{n_1(\theta,\phi)}{\lambda_1}-\frac{1}{\Lambda_{\text{eff}}(\theta,\phi)}=0. \quad (1)$$

θ and ϕ are the spherical angles in the dielectric frame (x,y,z). λ_1, λ_2 and λ_3 are the wavelengths of the interacting waves that verify the energy conservation $\lambda_3^{-1}=\lambda_1^{-1}+\lambda_2^{-1}$; n_1, n_2 and n_3 are the corresponding refractive indices in the considered direction (θ,ϕ). $\Lambda_{\text{eff}}(\theta,\phi)=\Lambda|\sin(\theta)\cos(\phi)|^{-1}$ is the effective grating periodicity in the direction (θ,ϕ) that ranges from Λ along the x axis to infinity when propagation occurs in the yz plane. Note that this latest case corresponds to birefringence phase matching, for which there is no grating. From the implication of $\Lambda_{eff}(\theta,\phi)$ in Eq. (1), AQPM authorizes the $2^3=8$ possible refractive indices combinations, defining the eight AQPM types, whereas birefringence phase matching allows only three of them [6].

To be able to measure any SHG or DFG AQPM direction, we cut a 5%MgO:PPLN crystal with a grating period $\Lambda=32.2$ μm as a sphere with a diameter of 3.9 mm. It was polished, oriented, and stuck on a goniometric head along the x or y axis with a precision better than 0.05° by using the Laue method. The sphere being placed at the center of an Euler circle, it was possible to propagate the laser beams in any direction of propagation of the crystal by keeping normal incidence. A focusing lens located at the entrance side of the sphere ensures a quasi-parallel propagation of the beams inside the sample. These beams are emitted by a parametric source from Excel Technology and Light Conversion that delivers 15 ps FWHM pulses at a 10 Hz repetition rate tunable between 0.4 and 10 μm. We used this tunable beam as the fundamental wave for SHG measurements. Furthermore, by mixing this beam with a beam at 1.064 μm, it was possible to study DFG. Two half-wave plates allowed the incident beams to be polarized according to the chosen AQPM type. The wavelengths were continuously controlled by a Chromex 250 SM monochromator. SHG or DFG directions are detected when the associated conversion efficiency is maximal, leading to measurement accuracy of about ±1°.

In the following, we use the notation SHG $(\lambda_\omega,\lambda_\omega,\lambda_{2\omega})$ for SHG $(\lambda_\omega^{-1}+\lambda_\omega^{-1}=\lambda_{2\omega}^{-1})$, and DFG

$(\lambda_p, \lambda_s, \lambda_i)$ for DFG $(\lambda_p^{-1} - \lambda_s^{-1} = \lambda_i^{-1})$, where λ_p, λ_s, and λ_i are the pump, signal, and idler wavelengths, respectively. By using the experimental setup described above we were able to measure the AQPM tuning curves at $T = 22°C$ of type I SHG $(\lambda_\omega^o, \lambda_\omega^o, \lambda_{2\omega}^e)$, type II $\equiv$ III SHG $(\lambda_\omega^o, \lambda_\omega^e, \lambda_{2\omega}^e)$, type I DFG $(\lambda_p^e, \lambda_s^e, \lambda_i^o)$, and type II DFG $(\lambda_p^e, \lambda_s^o, \lambda_i^e)$ in the full space of 5%MgO:PPLN, with indices (o) and (e) standing for the ordinary and extraordinary polarizations, respectively. The example of type I SHG is given in Fig. 1 in both the xz and the yz planes, while Fig. 2 shows types I and II DFG in the xz planes.

Our experimental data are well modelized by using Eq. (1) and the following Sellmeier equation with the coefficients of [7] given in Table 1,

$$n^i(\lambda) = \left(A^i + \frac{B^i}{\lambda^2 - C^i} - D^i \lambda^2 \right)^{1/2}, \qquad (2)$$

where $i = (o, e)$ is relative to the ordinary and extraordinary principal refractive indices.

Our experimental data allowed us to refine the Sellmeier equations of this material, thanks to a nonlinear least-squares fit, by using Eqs. (1) and (2), which led to a really much better agreement with our experimental data compared with calculations from Sellmeier equations of [7,8], as shown in Figs. 1 and 2. The corresponding Sellmeier coefficients are given in Table 1; they are the best set of coefficients for the considered sample. Since the precision of our measurements is ±1°, the new refractive indices have a typical accuracy $\Delta n^{o,e}/n^{o,e}$ better than 10^{-4} over the entire transparency range of the crystal, which can be easily verified by numerical calculations using Eq. (1).

From our refined Sellmeier equations, it is possible to have a reliable picture of the tunability of 5%MgO:PPLN. The example of SHG is given in Fig. 3, where the distance between the upper part and the lower part of the curves at a given Λ gives the maximum wavelength range that is accessible for a given type by varying the θ angle in the xz plane. Figure 3 shows that types I and II SHG are allowed for any value of Λ, while type IV SHG $(\lambda_\omega^e, \lambda_\omega^e, \lambda_{2\omega}^e)$ is possible only if $\Lambda \leqslant 24$ μm. Furthermore, we see that it is necessary to have $\Lambda \leqslant 13$ μm in order to reach $\lambda_\omega = 5.5$ μm that is the infrared cutoff wavelength of the

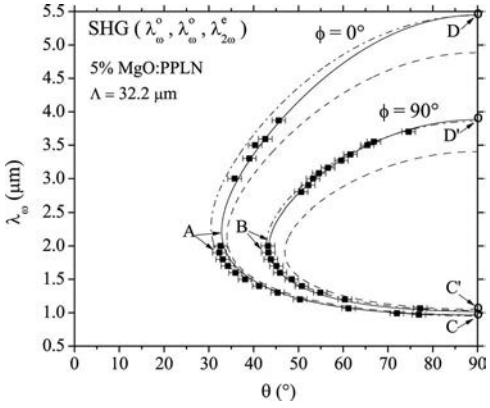

Fig. 1. Type I SHG AQPM tuning curves; the fundamental wavelength λ_ω is given as a function of θ at $\phi = 0°$ and $\phi = 90°$. Dots stand for experimental data, dashed and dashed-dotted curves correspond to calculations from Sellmeier equations of [7,8], respectively, and solid curves are the fits of the experimental data. Vertical tangents of the curves at points A and B correspond to spectrally noncritical interactions.

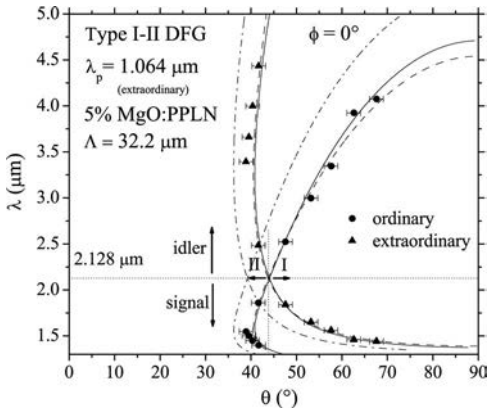

Fig. 2. Type I and II DFG AQPM tuning curves with a pump at 1.064 μm; λ stands for the signal or idler wavelengths plotted as a function of θ at $\phi = 0°$. Dots correspond to experimental data; dashed and dashed–dotted curves correspond to calculations from Sellmeier equations of [7,8], respectively, and the solid curves to the fit of the experimental data.

Table 1. Sellmeier Coefficients Relative to Ordinary (o) and Extraordinary (e) Principal Refractive Indices of 5%MgO:PPLN at $T = 22°C$

Sellmeier Coefficients	[7]	Present Work
A^o	4.87620	4.89789
B^o	0.11554	0.14720
C^o	0.04674	0.02719
D^o	0.03312	0.03305
A^e	4.54690	4.52222
B^e	0.09478	0.09194
C^e	0.04439	0.07475
D^e	0.02672	0.03647

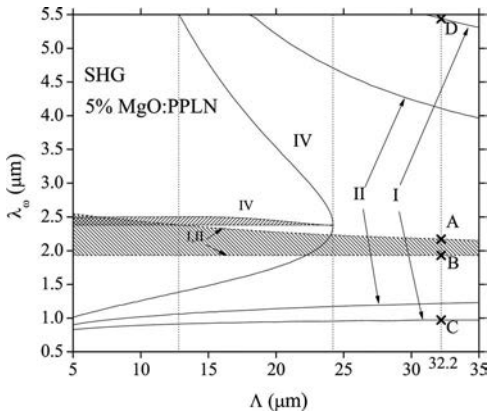

Fig. 3. Fundamental wavelength tuning ranges (solid curves) and maximal acceptance domains (hatched zones) of types I, II, and IV AQPM SHG calculated in the xz plane, as a function of the grating periodicity Λ. Dots A, B, C, and D refer to particular points of the tuning curves of Fig. 1.

crystal. For more legibility we did not plot the curves relative to types V ($\lambda^o_\omega,\lambda^o_\omega,\lambda^o_{2\omega}$), VI≡VII ($\lambda^o_\omega,\lambda^e_\omega,\lambda^o_{2\omega}$), and VIII ($\lambda^e_\omega,\lambda^e_\omega,\lambda^o_{2\omega}$) SHG; type V has a behavior comparable with that of type IV, and the other types are possible only at very small periodicities that are not yet accessible because of technological difficulties. Figure 3 shows that type I is the most favorable configuration for a broad wavelength tuning of SHG, even if the corresponding effective coefficient involving d_{22} and d_{31} is about seven times lower than d_{33} that governs type IV [1]. Concerning DFG, the same graphics that can be obtained by using Eqs. (1) and (2) and our Sellmeier coefficients given in Table 1 show that type I and type II are also the most favorable ones for wavelength tuning.

We also emphasize that AQPM presents interesting characteristics concerning the spectral acceptance. This is shown in Fig. 4, giving the example of type I SHG at ϕ=0° where the spectral acceptance $L\delta\lambda_\omega$ exhibits a maximum value of about 0.08 cm μm at λ_ω=2.22 μm; this particular wavelength corresponds to the vertical slope of the curve of Fig. 1 marked with dot A. By varying the ϕ angle from 0° to 90°, the wavelength associated with the vertical slope shifts until it reaches λ_ω=2.09 μm for ϕ=90°, which corresponds to dot B in Fig. 1. In this way, at Λ =32.2 μm, thanks to continuous variation of the ϕ angle, AQPM allows a continuous shift of the wavelength inside the interval 2.09 μm$<\lambda_\omega<$2.22 μm for which spectral acceptance is maximal. The hatched zones in Fig. 4 show how this interval increases as the grating period decreases and how types I and II exhibit domains that are complementary and wider than those of type IV. Such large spectral acceptance domains also exist for DFG and can be easily calculated by using the given Sellmeier equations.

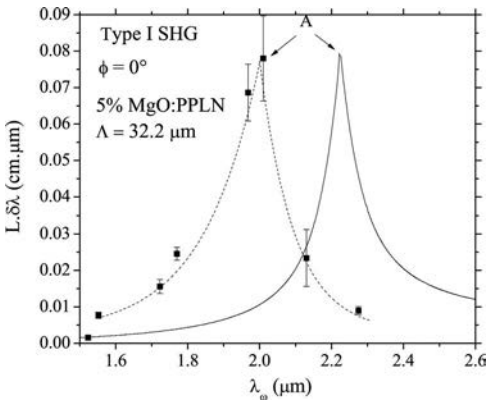

Fig. 4. Type I SHG AQPM spectral acceptance in the *xz* plane as a function of the fundamental wavelength λ_ω. Dots stand for experimental data; the dotted curve is a guide for the eyes, and the solid curve corresponds to calculations from the Sellmeier equations determined in the present work. The maximum, denoted A, corresponds to the vertical tangent of the curve of Fig. 1.

As a conclusion, we experimentally validated the theory of AQPM by reporting SHG and DFG measurements, which was one of our objectives. From these data we also proposed refined Sellmeier equations for 5%MgO:PPLN and showed that AQPM opens additional spectral ranges compared to birefringence phase matching and allows large spectral acceptances for a continuous wavelengths range. This feature is very interesting when considering parametric processes achieved in the femtosecond regime, for which a large spectral range needs to be simultaneously frequency converted to maintain ultrashort temporal pulse behavior for the generated beams [9]. Note that AQPM may also be interesting for PPKTP [2], PPLT [3], and PPKN [10], since they exhibit nonlinear coefficients with the same order of magnitude as those of PPLN.

References

1. M. M. Fejer, G. A. Magel, D. H. Jundt, and R. L. Byer, IEEE J. Quantum Electron. **28**, 2631 (1992).
2. H. Karlsson and F. Laurell, Appl. Phys. Lett. **71**, 3474 (1997).
3. F. Rotermund, J. Y. Chang, V. Petrov, F. Noack, S. Kurimura, N.-E. Yu, and K. Kitamura, Opt. Express **12**, 6421 (2004).
4. T. Skauli, K. L. Vodopyanov, T. J. Pinguet, A. Schober, O. Levi, L. A. Eyres, M. M. Fejer, J. S. Harris, B. Gerard, L. Becouarn, E. Lallier, and G. Arisholm, Opt. Lett. **27**, 628 (2002).
5. H. Ishizuki, T. Taira, S. Kurimura, J. H. Ro, and M. Cha, Jpn. J. Appl. Phys. Part 1 **42**, 108 (2003).
6. Y. Petit, B. Boulanger, P. Segonds, and T. Taira, Phys. Rev. A **76**, 063817 (2007).
7. Casix, "Lithium niobate crystal series," http://www.casix.com/product/prod_cry_linbo3. html.
8. O. Gayer, Z. Sacks, E. Galun, and A. Arie, Appl. Phys. B **91**, 343 (2008).
9. M. Beutler, M. Ghotbi, F. Noack, D. Brida, C. Manzoni, and G. Cerullo, Opt. Lett. **34**, 710 (2009).
10. J. P. Meyn, M. E. Klein, D. Woll, and R. Wallenstein, Opt. Lett. **24**, 1154 (1999).